

Evolution of near-inertial waves

By R. C. KLOOSTERZIEL AND P. MÜLLER

School of Ocean and Earth Science and Technology, University of Hawaii,
Honolulu, HI 96822, USA

(Received 3 June 1994 and in revised form 15 June 1995)

The three-dimensional evolution of near-inertial internal gravity waves is investigated for the case of a laterally unbounded fluid layer of constant finite depth. A general Green's function formulation is derived which can be used to solve initial value problems or study the effect of forcing. The Green's function is expanded in vertical normal modes, and is very singular. Convolutions with finite-sized initial conditions lead however to well-behaved solutions. Expansions in similarity solutions of the diffusion equation are shown to be an alternative for finding exact solutions to initial value problems, with respect to one normal mode. For the case of constant buoyancy frequency normal modes expansions are shown to be equivalent to expansions in an alternative series of which the first term is the response on the infinite domain, all the others being corrections to account for the no-flux boundary condition on the upper and lower boundaries.

1. Introduction

In this paper we study the evolution or dispersion of near-inertial internal gravity wave packets by analytical and semi-analytical means. Near-inertial internal gravity waves are a major component of the oceanic internal wave field. Kinetic energy spectra in the ocean nearly always show a pronounced 'inertial peak' at frequencies slightly above the Coriolis frequency (e.g. Fu 1981). Near-inertial internal waves in the upper ocean are thought to be generated by fluctuations in the atmospheric windstress. These fluctuations cause inertial oscillations in the oceanic surface mixed layer. Part of their energy leaks into the underlying ocean as near-inertial internal waves. An open question is what processes actually cause the leakage. True inertial oscillations with frequencies right at the Coriolis frequency have an infinite horizontal scale and do not exert a pressure force on the underlying ocean. For leakage to occur, some process is needed that imposes a finite horizontal scale and shifts the frequency above the Coriolis frequency. The finite size of the atmospheric disturbance, lateral variations of the oceanic waveguide (e.g. Coriolis frequency, buoyancy frequency, ocean depth) and mean currents are the prime candidates. Here we look at the evolution of near-inertial internal waves after the passing of a finite-sized atmospheric disturbance or equivalently at the evolution of a finite-sized wave packet in an otherwise homogeneous ocean.

The near-inertial oceanic response to atmospheric storms or disturbances has been extensively studied (e.g. Pollard 1970; Greatbatch 1983, 1984; Price 1983; Rubenstein 1983; Gill 1984; Kundu & Thomson 1985; Kundu 1993). These oceanographic studies were aimed at determining the response and at estimating how much near-inertial energy leaks from the surface mixed layer into the underlying ocean. The effects

of nonlinearity, mixing, β -effect and size and horizontal speed of the atmospheric disturbance was considered. The study closest to ours is Gill (1984) who studied the dispersion of near-inertial waves in the wake of a storm. His initial conditions were invariant in the x -direction (the storm track), and either periodic in the y -direction or confined to a narrow band. In the latter case the calculations were done numerically and involved summing up a number of normal modes. Gill showed that the initial loss of energy from the surface mixed layer may be a major contributor to the internal wave energy in the underlying thermocline. He also showed that the amplitude of the near-inertial waves is intermittent, that vertical scales tend to decrease with time, and that there is some bottom intensification of energy. In the y -periodic case the problem becomes that of dispersion in the vertical only, with a fixed horizontal structure. Our study differs from Gill's study in that we look at the horizontal dispersion of a single normal mode and the simultaneous horizontal and vertical dispersion. More importantly, our study differs because we calculate the dispersion in an analytical or semi-analytical way.

The dispersion relation of near-inertial internal gravity waves has a peculiar behaviour. In the horizontal, small-scale waves propagate the fastest, whereas in the vertical large-scale waves propagate the fastest. Furthermore, the horizontal and vertical group velocities approach zero as the frequency of the waves approaches the Coriolis frequency. The dispersion problem is part of the Rossby adjustment problem (Gill 1982). Any initial condition can be decomposed into a geostrophically balanced part and a gravity part. The geostrophic part carries the potential vorticity of the flow. The gravity part disperses in the form of surface and internal gravity waves, leaving behind the geostrophically balanced part. We only consider the baroclinic adjustment problem here. For storm sizes $O(500 \text{ km})$ only the baroclinic part of the flow field adjusts by the dispersion of near-inertial internal gravity waves. The barotropic part adjusts much faster by much higher frequency surface gravity waves.

In §2 we derive the equation that governs the evolution of baroclinic near-inertial internal waves. This derivation makes essential use of the fact that the scale of near-inertial waves is much larger than the Rossby radius of deformation, i.e. that the Burger number is much smaller than 1. For scales $O(500 \text{ km})$ this is only true for the baroclinic modes (the baroclinic Rossby radii in the ocean are $O(50 \text{ km})$ or less) but not for the barotropic mode (the barotropic Rossby radius is typically $O(2000 \text{ km})$ at mid-latitudes). The resulting equation is an integro-differential equation for a complex amplitude which is first order in time. Our derivation of this equation is somewhat *ad hoc*. A much more systematic, but also much more involved derivation is given in Hasselmann (1970) using projection operators that decompose the flow field into its geostrophic and gravity component. This projection operator formalism does not require the Burger number to be small.

The Green's function is determined in §3. It is singular at the time origin, because large horizontal wavenumbers propagate with unbounded speed in the small Burger number approximation used here. This singular behaviour causes no problems however once initial conditions are used that have vanishing energy at high wavenumbers. Formally, the Green's function can be used to find the solution for any initial wave-field distribution, and can also be used to determine the evolution for problems with forcing included. In Appendix A we show that initial value problems can also be solved by an expansion into similarity solutions, in close analogy to Kloosterziel's (1990) results for the diffusion equation. In §4 we narrow our focus to the case of constant Brunt-Väisälä frequency. In that case there is an alternative to using normal modes expansions. With the Poisson sum formula, a normal modes series can

be converted into a different series which has a simple physical interpretation when the evolution of an approximate point source is considered. The first term in this alternative series gives the evolution of a point source in infinite space, while all the other terms are strategically located point sources ('image points' analogous to 'image charges' found in electrostatics problems) which ensure that the boundary conditions on the finite vertical domain are satisfied. They can be thought of as describing the reflections of the waves at the boundaries. The Poisson converted series converges far more rapidly than a normal modes expansion, that is, few terms are needed to get a reliable picture of the evolution. As an example we finally apply the Poisson conversion to the case of an initial condition which is Gaussian in the horizontal and which has a large amplitude in a narrow layer near the surface. Many normal modes need to be summed here at any time, except for at large horizontal distances where the propagation of the first baroclinic mode dominates. With the Poisson sum formula we obtain an alternative series which converges rapidly for large time at small and intermediate distances from the centre. Section 5 summarizes the main results. Oceanographic implications of our results will be published elsewhere as well as many details of the wavefield evolution in various cases, omitted here for the sake of brevity.

2. Equations of motion

Consider linear hydrostatic motions of an incompressible rotating stratified Boussinesq fluid in an unbounded ocean of constant depth H . Their governing equations are

$$\partial_t u - f_0 v + \partial_x p = 0, \tag{1}$$

$$\partial_t v + f_0 u + \partial_y p = 0, \tag{2}$$

$$-b + \partial_z p = 0, \tag{3}$$

$$\partial_t b + N^2(z)w = 0, \tag{4}$$

$$\partial_x u + \partial_y v + \partial_z w = 0, \tag{5}$$

together with the boundary conditions

$$\partial_t \zeta = w \text{ at } z = 0, \tag{6}$$

$$p = g\zeta \text{ at } z = 0, \tag{7}$$

$$w = 0 \text{ at } z = -H. \tag{8}$$

Here u, v and w are the zonal, meridional and vertical velocity components, respectively, p the pressure (divided by a reference density), f_0 the constant Coriolis frequency, b the buoyancy, $N^2(z)$ the Brunt-Väisälä or buoyancy frequency, and ζ the free-surface elevation. The surface is at $z = 0$ and the bottom at $z = -H$. With (5) and the boundary condition (8) we have

$$w = - \int_{-H}^z (\partial_x u + \partial_y v) dz', \tag{9}$$

and using (3) to eliminate b , the buoyancy equation (4) can be written as

$$\partial_z \partial_t p = N^2(z) \int_{-H}^z (\partial_x u + \partial_y v) dz', \tag{10}$$

with boundary condition (this follows from (6) and (7))

$$\partial_t p = gw \quad \text{at } z = 0. \quad (11)$$

Equation (10) is integrated in conjunction with this boundary condition and (9) to yield

$$\partial_t p = - \int_z^0 dz' N^2(z') \int_{-H}^{z'} dz'' (\partial_x u + \partial_y v) - g \int_{-H}^0 dz'' (\partial_x u + \partial_y v). \quad (12)$$

The equations of motion can therefore be rewritten in the matrix form (Hasselmann 1970)

$$\partial_t \begin{pmatrix} u_+ \\ u_- \\ p \end{pmatrix} + \begin{pmatrix} if_0 & 0 & \partial_+ \\ 0 & -if_0 & \partial_- \\ \frac{1}{2}f_0^2 \mathcal{J} \partial_- & \frac{1}{2}f_0^2 \mathcal{J} \partial_+ & 0 \end{pmatrix} \begin{pmatrix} u_+ \\ u_- \\ p \end{pmatrix} = 0, \quad (13)$$

where

$$u_{\pm} = u \pm iv, \quad \partial_{\pm} = \partial_x \pm i\partial_y, \quad (14)$$

are the rotary components of the horizontal velocity vector and the gradient operator, respectively, and

$$\mathcal{J} = \int_z^0 dz' \frac{N^2(z')}{f_0^2} \int_{-H}^{z'} dz'' + \frac{g}{f_0^2} \int_{-H}^0 dz''. \quad (15)$$

The equation for u_- is the complex conjugate of that for u_+ .

The integral operator \mathcal{J} defines the vertical eigenvalue problem

$$\mathcal{J} \phi_n(z) = R_n^2 \phi_n(z), \quad (16)$$

where $\phi_n(z)$ ($n = 0, 1, 2, \dots$) is a denumerably infinite set of vertical eigenfunctions (normal modes) and R_n^2 the associated eigenvalues. R_n is called the n th Rossby radius of deformation. The eigenvalue problem (16) is equivalent to the usual differentiated form

$$\frac{d}{dz} \frac{f_0^2}{N^2(z)} \frac{d}{dz} \phi_n + \frac{1}{R_n^2} \phi_n = 0, \quad (17)$$

with the homogeneous boundary conditions

$$\left. \frac{d\phi_n}{dz} \right|_{z=-H} = 0, \quad g \left. \frac{d\phi_n}{dz} + N^2 \phi_n \right|_{z=0} = 0 \quad (18)$$

(see Gill 1982). Note that the boundary conditions are accounted for by the integral operator, while in the differential form they have to be explicitly stated. The magnitude of the Rossby radii decreases monotonically with increasing mode number n . The Rossby radius R_0 of the zeroth or external mode is several orders of magnitude larger than the radii for the internal modes $n = 1, 2, \dots$. The ratio is approximately $R_0^2/R_n^2 = n^2 \pi^2 g/HN^2$ which is $O(n^2 \times 10^3)$ for typical deep ocean conditions.

Eigenfunctions of \mathcal{J} are used to find solutions to (13) with separable z -dependency. For instance, in a horizontally unbounded ocean equation (13) has plane wave solutions

$$\begin{pmatrix} u_+(x, y, z; t) \\ u_-(x, y, z; t) \\ p(x, y, z; t) \end{pmatrix} = a_{k,n,s} \begin{pmatrix} U_+^{k,n,s} \\ U_-^{k,n,s} \\ P^{k,n,s} \end{pmatrix} \phi_n(z) \exp(i(kx + ly - \omega_{k,n,s}t)), \quad (19)$$

where $\mathbf{k} = (k, l)$ is the horizontal wavenumber vector, n is the vertical mode number,

$s = 0, +, -$ the wavebranch index, $a_{k,n,s}$ the wave amplitudes, $(U_+^{k,n,s}, U_-^{k,n,s}, P^{k,n,s})$ the polarization vector, and $\omega_{k,n,s}$ the frequency given by the dispersion relation

$$\omega_{k,n,s} = sf_0(1 + |\mathbf{k}|^2 R_n^2)^{1/2}, \quad |\mathbf{k}|^2 = k^2 + l^2. \tag{20}$$

Here $s = 0$ represents the steady, quasi-geostrophically balanced ‘wave’ branch (zero frequency) and $s = +, -$ the two gravity wave branches. Explicit expressions for the polarization vectors are given in Hasselmann (1970); they will not be needed in the present paper.

Any solution to (13) can be decomposed into the three wave branches, even if the horizontal and vertical structure is not resolved into normal modes. The decomposition requires finding the eigenvectors and eigenfrequencies of the matrix in (13). When the spatial structure is not resolved these eigenvectors and eigenfrequencies are operators. The decomposition then takes the form

$$\begin{pmatrix} u_+(x, y, z; t) \\ u_-(x, y, z; t) \\ p(x, y, z; t) \end{pmatrix} = \sum_s \begin{pmatrix} U_+^s \\ U_-^s \\ P^s \end{pmatrix} a^s(x, y, z; t), \tag{21}$$

where (U_+^s, U_-^s, P^s) is the eigen- or polarization vector (operator) and $a^s(x, y, z; t)$ the wave branch amplitudes. The equation of motion for the wavebranch amplitudes is obtained by substituting (21) in (13) and applying the adjoint eigen- or polarization operator. The result is

$$\partial_t a^s(x, y, z; t) + i\Omega^s a^s(x, y, z; t) = 0, \tag{22}$$

where Ω^s is the eigenfrequency operator. The actual algebra is involved and given in Hasselmann (1970). The decomposition can also be performed if source terms (forcing) are added to the right-hand side of (13). Then a source term also appears on the right-hand side of (22).

The complexities of Hasselmann’s analysis can be circumvented since we only consider the internal Rossby adjustment process due to the dispersion of the relatively slow internal modes and not the external adjustment due to the dispersion of the fast external surface mode. For internal modes the rigid lid approximation $w = 0$ at $z = 0$ can be imposed. Equation (9) then implies that u, v are baroclinic and (1) and (2) then imply that the vertical average of the pressure is zero. Integration of (10) from $z' = z$ to $z' = 0$ yields an integration constant which is determined by this condition, and we find

$$\partial_t p = - \int_z^0 dz' N^2(z') \int_{-H}^{z'} dz'' (\partial_x u + \partial_y v) + \frac{1}{H} \int_{-H}^0 dz \int_z^0 dz' N^2(z') \int_{-H}^{z'} dz'' (\partial_x u + \partial_y v). \tag{23}$$

Thus, if we restrict ourselves to the internal or baroclinic dispersion then the operator \mathcal{J} in (13) needs to be replaced by

$$\mathcal{L} = \left(1 - \frac{1}{H} \int_{-H}^0 dz \right) \int_z^0 dz' \frac{N^2(z')}{f_0^2} \int_{-H}^{z'} dz'' \tag{24}$$

and the integral eigenvalue problem becomes

$$\mathcal{L} \phi_n = R_n^2 \phi_n,$$

which yields the same eigenmodes as (17) with boundary conditions

$$\left. \frac{d\phi_n}{dz} \right|_{z=-H,0} = 0, \quad n = 1, 2, \dots \quad (25)$$

but not the barotropic mode ($n = 0$). The eigenmodes are all baroclinic, i.e.

$$\int_{-H}^0 \phi_n(z) dz = 0, \quad n = 1, 2, \dots$$

(conversely, integration of (17) shows that $d_z \phi_n = 0$ at $z = -H$ and baroclinicity implies $d_z \phi_n = 0$ at $z = 0$).

The second approximation that we employ is based on the assumption that the Burger number

$$B = \frac{|\mathcal{L}|}{L^2} \approx \frac{N_0^2 H^2}{f_0^2 L^2} \quad (26)$$

is much smaller than one. Here N_0 is a typical value of the Brunt–Väisälä frequency, and L a typical horizontal lengthscale of the wavefield. The small Burger number approximation is a long-wave approximation, i.e. we consider motions that vary in the horizontal on a scale which is large compared to the depth H of the fluid and such that H/L multiplied by $|N_0/f_0|$ is small. To derive the equation of motion in the small Burger number limit, consider the complex amplitude

$$a^+(x, y, z; t) = u_+ - \frac{i}{f_0} \partial_+ p + \frac{1}{4} \mathcal{L} \partial_+ (\partial_- u_+ - \partial_+ u_-). \quad (27)$$

The second and the third terms on the right-hand side are of the order of the Burger number. For the third term this is obvious. To see this is the case for the second term we recall that for pure inertial oscillations ($B = 0$) the pressure vanishes. From (13) we find the evolution for a^+ to be

$$\partial_t a^+ = -if_0 a^+ + if_0 \frac{1}{2} \mathcal{L} \partial_+ \partial_- u_+ = -if_0 a^+ + if_0 \frac{1}{2} \mathcal{L} \partial_+ \partial_- a^+ + O(B^2). \quad (28)$$

Correct to first order in the Burger number B the near-inertial amplitude evolves according to

$$\partial_t a^+ + if_0 a^+ - i \frac{1}{2} f_0 \nabla_h^2 \mathcal{L} a^+ = 0, \quad (29)$$

where

$$\nabla_h^2 = \partial_+ \partial_- = \partial_x^2 + \partial_y^2 \quad (30)$$

is the horizontal Laplace operator. Vertical integration of (29) using (24) shows that the field is at all times baroclinic, i.e.

$$\int_{-H}^0 a^+ dz = 0, \quad (31)$$

if it is initially. Equation (29) can also be obtained by applying Hasselmann's (1970) projection formalism which yields

$$\partial_t a^+ + if_0 (1 - \mathcal{L} \partial_+ \partial_-)^{1/2} a^+ = 0, \quad (32)$$

for arbitrary Burger number. The small Burger number limit we consider here, i.e. (29), is obtained by expanding the square root in (32). When vertical and horizontal normal modes like (19) are introduced, equation (32) reproduces the dispersion relation (20) and equation (29) the dispersion relation

$$\omega_{k,n,+} = f_0 (1 + \frac{1}{2} |\mathbf{k}|^2 R_n^2), \quad (33)$$

which is the correct approximation for $|\mathbf{k}|^2 R_n^2 \ll 1$, i.e. for waves with small enough horizontal wavenumbers, i.e. large horizontal scales. In this approximation the horizontal group velocity c_g has for a given vertical normal mode a magnitude

$$|c_g| = |f_0| |\mathbf{k}| R_n^2, \tag{34}$$

which is unbounded for $|\mathbf{k}| \rightarrow \infty$, while without the small Burger number approximation the group velocity

$$|c_g| = \frac{|f_0| |\mathbf{k}| R_n^2}{(1 + |\mathbf{k}|^2 R_n^2)^{1/2}} \tag{35}$$

has an upper bound $|f_0| R_n$.

Equation (29) is equivalent to the differential form

$$(\partial_t + if_0) \frac{\partial}{\partial z} \frac{f_0^2}{N^2(z)} \frac{\partial a^+}{\partial z} + \frac{1}{2} if_0 \nabla_h^2 a^+ = 0, \tag{36}$$

with the conditions

$$\partial_z a^+ \Big|_{z=-H,0} = 0. \tag{37}$$

The evolution of the complex conjugate of a^+ , denoted by a^- , is governed by the complex conjugate of (29)

$$\partial_t a^- - if_0 a^- + i \frac{1}{2} f_0 \mathcal{L} \nabla_h^2 a^- = 0, \tag{38}$$

where $a^- = (a^+)^*$ (a^* denotes complex conjugate). If we multiply (29) by a^- and (38) by a^+ and add, we obtain

$$\partial_t a^+ a^- = \partial_t |a^+|^2 = i \frac{1}{2} f_0 (a^- \mathcal{L} \nabla_h^2 a^+ - a^+ \mathcal{L} \nabla_h^2 a^-). \tag{39}$$

It is not hard to show that \mathcal{L} is a self-adjoint integral operator, that is $\int_{-H}^0 \phi \mathcal{L} \psi dz = \int_{-H}^0 \psi \mathcal{L} \phi dz$, if ϕ, ψ satisfy $\int_{-H}^0 \phi dz = \int_{-H}^0 \psi dz = 0$, which is the condition to be satisfied by a^\pm (baroclinicity). Therefore, we have

$$\int_{-H}^0 (a^- \mathcal{L} \nabla_h^2 a^+ - a^+ \mathcal{L} \nabla_h^2 a^-) dz = \nabla_h \cdot \int_{-H}^0 ((\mathcal{L} a^-) \nabla_h a^+ - a^+ \nabla_h \mathcal{L} a^-) dz, \tag{40}$$

with

$$\nabla_h = i \partial_x + j \partial_y. \tag{41}$$

When we integrate (39) over the (x, y) -plane, we find that

$$\frac{d}{dt} \int \int \int_{-H}^0 |a^+|^2 dz dx dy = 0, \tag{42}$$

if

$$\left| \int_{-H}^0 ((\mathcal{L} a^-) \nabla_h a^+ - a^+ \nabla_h \mathcal{L} a^-) dz \right|$$

goes to zero ‘fast enough’ as $|x, y| \rightarrow \infty$. To lowest order in the Burger number $|a^+|^2/2$ is equal to the horizontal kinetic energy density.

We scale the vertical coordinate by the fluid layer depth H , the horizontal coordinates with some arbitrary lengthscale L , time with f_0^{-1} and $N(z)$ by some typical value N_0 . The non-dimensional form of (29) is then

$$\partial_t a^+ + ia^+ - i \frac{1}{2} \varepsilon \mathcal{L} \nabla_h^2 a^+ = \rho^+, \tag{43}$$

where \mathcal{L} and ∇_h^2 are now dimensionless and

$$\varepsilon = \frac{N_0^2 H^2}{f_0^2 L^2} \tag{44}$$

the Burger number. On the right-hand side of (43) the term ρ^+ represents all possible baroclinic forcing terms. Integration of (43) in the vertical shows that a^+ remains baroclinic if it so initially and if ρ^+ is baroclinic at all times.

3. Green's function

3.1. Baroclinic Green's function

In this section we derive the appropriate Green's function formulation for the general problem where forcing and initial conditions are supplied. Although we will focus on the initial value problem in the present paper, the general expression is derived here for future reference purposes. The conjugate version of (43) for the Green's function is

$$\begin{aligned} -\partial_{t_0} G(\mathbf{r}, t | \mathbf{r}_0, t_0) + iG(\mathbf{r}, t | \mathbf{r}_0, t_0) - i\frac{1}{2}\varepsilon \mathcal{L}_0 \nabla_{h0}^2 G(\mathbf{r}, t | \mathbf{r}_0, t_0) \\ = \delta(t - t_0) [\delta(z - z_0) - 1] \delta(x - x_0) \delta(y - y_0), \end{aligned} \tag{45}$$

where $G = 0$ for $t_0 > t$ (causality). Here the δ denote Dirac delta functions. The index 0 is affixed to the integral operator to indicate that it acts on the z_0 -dependent part of the Green's function. The variables with the index 0 represent 'source' space-time coordinates while the variables without an index correspond to observer coordinates. The reason for the use of a term $\delta(z - z_0) - 1$ instead of just $\delta(z - z_0)$ is that we will seek an expansion of G in vertical normal modes, which are baroclinic. This is only possible if the right-hand side of (45) can also be expanded in a similar fashion, and this requires a 'baroclinic' delta function. To simplify the notation we have indicated a triplet of spatial Cartesian coordinates in vector notation by

$$\mathbf{r}_{(0)} = i x_{(0)} + j y_{(0)} + k z_{(0)}.$$

When we integrate (45) from $t_0 = t - \Delta t$ to $t_0 > t$, with $\Delta t > 0$ arbitrarily small, we find $G(\mathbf{r}, t | \mathbf{r}_0, t_0 = t) = [\delta(z - z_0) - 1] \delta(x - x_0) \delta(y - y_0)$, or, in other words, G describes the evolution of a (baroclinic) point source which is released at $t_0 = t$.

When we take $G \times (43) - a^+ \times (45)$, we get

$$\begin{aligned} G(\mathbf{r}, t | \mathbf{r}_0, t_0) \partial_{t_0} a^+(\mathbf{r}_0; t_0) + a^+(\mathbf{r}_0; t_0) \partial_{t_0} G(\mathbf{r}, t | \mathbf{r}_0, t_0) + i\frac{1}{2}\varepsilon a^+(\mathbf{r}_0; t_0) \mathcal{L}_0 \nabla_{h0}^2 G(\mathbf{r}, t | \mathbf{r}_0, t_0) \\ - i\frac{1}{2}\varepsilon G(\mathbf{r}, t | \mathbf{r}_0, t_0) \mathcal{L}_0 \nabla_{h0}^2 a^+(\mathbf{r}_0; t_0) \\ = \rho^+(\mathbf{r}_0; t_0) G(\mathbf{r}, t | \mathbf{r}_0, t_0) - a^+(\mathbf{r}_0; t_0) \delta(t - t_0) [\delta(z - z_0) - 1] \delta(x - x_0) \delta(y - y_0). \end{aligned} \tag{46}$$

The first two terms combine into a single time derivative while the next two terms can be written as a divergence

$$i\frac{1}{2}\varepsilon \int_{-1}^0 (a^+ \mathcal{L}_0 \nabla_{h0}^2 G - G \mathcal{L}_0 \nabla_{h0}^2 a^+) dz_0 = i\frac{1}{2}\varepsilon \nabla_{h0} \cdot \int_{-1}^0 ((\mathcal{L}_0 a^+) \nabla_{h0} G - G \nabla_{h0} \mathcal{L}_0 a^+) dz_0, \tag{47}$$

if a^+ is baroclinic and if in addition

$$\int_{-1}^0 G(x, y, z, t | x_0, y_0, z_0, t_0) dz_0 = \int_{-1}^0 G(x, y, z, t | x_0, y_0, z_0, t_0) dz = 0, \tag{48}$$

because \mathcal{L} is then a self-adjoint integral operator (see remark at the end of §2). In (47) ∇_{h0} is given by (41) but with an index 0 attached to x, y .

Consider the problem where at $t = 0$ the field a^+ is specified and the forcing is given for $t \geq 0$. Integrating from $t_0 = 0$ to $t_0 = t^+$ and over space, the right-hand side of (3.1) is equal to

$$\int_0^{t^+} \int \int \int \rho^+(\mathbf{r}_0; t_0) G(\mathbf{r}, t | \mathbf{r}_0, t_0) dx_0 dy_0 dz_0 dt_0 - a^+(\mathbf{r}; t) + \int_{-1}^0 a^+(x, y, z_0; t) dz_0.$$

Since a^+ has to be baroclinic, the last integral is zero at all times. The divergence (47) when integrated over x_0, y_0 is zero if $|\nabla_{h0} G|$ and $|G|$ tend to zero fast enough (for all z_0) as $x_0^2 + y_0^2 \rightarrow \infty$. This needs to be verified later on, once G has been determined. Using the fact that $G(\mathbf{r}, t | \mathbf{r}_0, t_0) = 0$ for $t_0 > t$ we obtain

$$a^+(\mathbf{r}; t) = \int_{-1}^0 \int \int G(\mathbf{r}, t | \mathbf{r}_0, t_0 = 0) a^+(\mathbf{r}_0; t_0 = 0) dx_0 dy_0 dz_0 + \int_0^{t^+} \int_{-1}^0 \int \int \rho^+(\mathbf{r}_0; t_0) G(\mathbf{r}, t | \mathbf{r}_0, t_0) dx_0 dy_0 dz_0 dt_0. \tag{49}$$

3.2. Normal modes expansion

The Green's function for the finite-layer-depth case can be expressed as a series with respect to the vertical normal modes in the following fashion. One starts by expanding the $\delta(z - z_0) - 1$ term on the right-hand side of (45) in terms of the eigenfunctions of the operator \mathcal{L} . In the case of constant N^2 the eigenfunctions are for example

$$\phi_n(z) = \sqrt{2} \cos(n\pi z). \tag{50}$$

In this particular case it is clear that we can apply the usual Fourier theorems to expand z -dependent square-integrable functions in a cosine series. But, in general the eigenfunctions of \mathcal{L} are orthogonal and complete in an L_2 sense (see Morse & Feshbach, 1953). Therefore an arbitrary $\phi(z)$, which is square-integrable and which satisfies the same conditions as the eigenfunctions, can be developed in a series $\phi(z) = \sum_n \varpi_n \phi_n$, where $\varpi_n = (\phi, \phi_n)$ and $(f, g) = \int_{-1}^0 f g dz$. The eigenfunctions are normalized such that $(\phi_n, \phi_m) = \delta_{nm}$, with δ_{nm} the Kronecker δ symbol. Specifically

$$\delta(z - z_0) - 1 = \sum_{n=1}^{\infty} \phi_n(z) \phi_n(z_0). \tag{51}$$

We expand G in the same fashion:

$$G(x, y, z, t | x_0, y_0, z_0, t_0) = \sum_{n=1}^{\infty} G_n(x, y, t | x_0, y_0, t_0) \phi_n(z) \phi_n(z_0). \tag{52}$$

Substitution of (51) and (52) in (45) shows that G_n satisfies

$$-\partial_{t_0} G_n + i G_n - i \frac{1}{2} \varepsilon_n \nabla_{h0}^2 G_n = \delta(t - t_0) \delta(x - x_0) \delta(y - y_0). \tag{53}$$

Here the non-dimensional parameter ε_n is (the square of the non-dimensionalized n th Rossby radius)

$$\varepsilon_n = \frac{R_n^2}{L^2}. \tag{54}$$

The normal modes expansion implies that (48) is satisfied. Writing

$$\delta(x - x_0) = \frac{1}{2\pi} \int_{-\infty}^{+\infty} e^{ik(x-x_0)} dk, \quad \delta(y - y_0) = \frac{1}{2\pi} \int_{-\infty}^{+\infty} e^{il(y-y_0)} dl,$$

and putting

$$G_n = \frac{1}{2\pi} \int_{-\infty}^{+\infty} \int_{-\infty}^{+\infty} \gamma_n(k, l, t, t_0) e^{ik(x-x_0)} e^{il(y-y_0)} dk dl,$$

we find with (53) that γ_n satisfies

$$\partial_{t_0} \gamma_n - i\gamma_n - i\frac{1}{2}\epsilon_n(k^2 + l^2)\gamma_n = -\frac{1}{2\pi} \delta(t - t_0),$$

which is solved by

$$\gamma_n = \frac{U(t - t_0) e^{-i(t-t_0)}}{2\pi} e^{-i\frac{1}{2}(k^2+l^2)\epsilon_n(t-t_0)}.$$

Here $U(x)$ is the Heaviside stepfunction. For $t > t_0$ we have

$$G_n = \frac{e^{-i(t-t_0)}}{(2\pi)^2} \int_{-\infty}^{+\infty} e^{i(-k^2\epsilon_n(t-t_0)/2+k(x-x_0))} dk \int_{-\infty}^{+\infty} e^{i(-l^2\epsilon_n(t-t_0)/2+l(y-y_0))} dl. \tag{55}$$

Combining the k and l integrals, which are easy to evaluate, we find

$$G_n = U(t - t_0) \frac{\exp(iR^2/[2\epsilon_n(t - t_0)] - i(t - t_0))}{i2\pi\epsilon_n(t - t_0)}, \tag{56}$$

where R is the horizontal distance to the source point

$$R = ((x - x_0)^2 + (y - y_0)^2)^{1/2}. \tag{57}$$

Substitution of (56) in (52) yields the Green's function expanded in a series of vertical baroclinic modes.

For $t \downarrow t_0$ the G_n should tend to $\delta(x - x_0)\delta(y - y_0)$. It is not hard to show that we have

$$\lim_{t \downarrow t_0} \int_{x_0-\Delta x}^{x_0+\Delta x} \int_{y_0-\Delta y}^{y_0+\Delta y} G_n(x, y, t|x_0, y_0, t_0) dx dy = 1,$$

for any $\Delta x, \Delta y$, which is a defining property of δ -functions. For t close to t_0 the amplitude of G_n is everywhere large and oscillatory, and does *not* decay at infinity. This is a consequence of the small Burger number approximation which allows for unlimited group velocity (see (34)). Since waves of all wavelengths are used in equal measure to build up the δ -source, a signal can propagate with infinite velocity. At a fixed time (see figure 1a) shorter waves are found at larger distances from the source origin, which is in accordance with the dispersion relation (33) (shorter waves have higher group velocity). At a fixed point in space (see figure 1b), as a function of time, one first observes very rapid oscillations with an initially large amplitude. The amplitude decays with $1/t$ while the oscillation frequency decreases. Note that apart from the pure inertial part, time is scaled in each G_n by ϵ_n . The value of ϵ_n decreases with increasing n , because in (54) the Rossby radii R_n decrease with n , and therefore the evolution associated with higher vertical normal modes is slower than that of the lower modes. The fastest evolution is for the first baroclinic mode.

Although the G_n , and thus G , violate the assumption of vanishing at infinity, (49) is valid. Below, this will be shown through an example. There are various other ways to show the validity of (49), for instance with either Laplace transform or Fourier transform techniques.

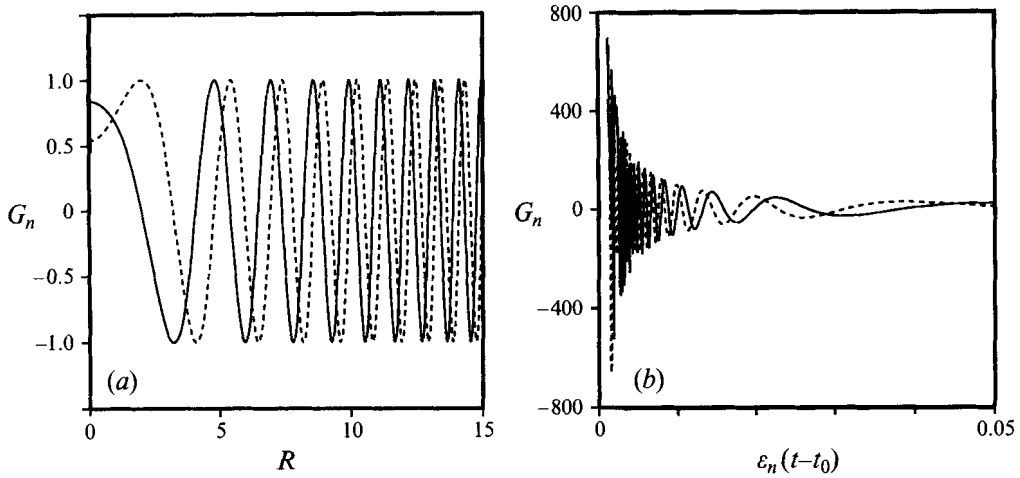


FIGURE 1. Graphs showing the real (solid lines) and imaginary part (dashed lines) of the Green's function G_n , as given by (56). (a) G_n as a function of R (horizontal distance to the source) at the non-dimensional time $\varepsilon_n(t - t_0) = 1$. (b) G_n as a function of time at a fixed position $R = 1$. Here, for $\varepsilon_n(t - t_0)$ near zero the graph has been cut off because the response becomes infinitely large with infinitely high frequency.

3.3. Example

The singular behaviour of the Green's function (infinite response everywhere near $t = t_0$) disappears when convoluted with initial conditions that have vanishing energy at the high horizontal wavenumbers, which is necessary for the small Burger number approximation to be valid (long-wave approximation). We will show this through a simple example here. According to (49) the evolution of an arbitrary initial condition $a^+(x, y, z; t = 0)$ is

$$a^+(x, y, z; t) = \sum_{n=1}^{\infty} a_n^+(x, y; t)\phi_n(z), \tag{58}$$

with

$$a_n^+(x, y; t) = \iint G_n(x, y, t|x_0, y_0, t_0 = 0)a_n^+(x_0, y_0; t = 0)dx_0 dy_0, \tag{59}$$

with G_n given by (56) and

$$a_n^+(x, y; t = 0) = \int_{-1}^0 a^+(x, y, z; t = 0)\phi_n(z)dz, \tag{60}$$

i.e. the projection of the initial condition on the n th mode. The evolution equation for a_n^+ is the projection of equation (43) on the n th mode (without forcing)

$$\partial_t a_n^+ + ia_n^+ - i\frac{1}{2}\varepsilon_n \nabla_h^2 a_n^+ = 0. \tag{61}$$

For instance consider the projected initial condition

$$a_n^+(x, y; t = 0) = \frac{e^{-(x^2+y^2)/2\alpha^2}}{2\pi\alpha^2}. \tag{62}$$

With (59) the evolution is

$$a_n^+(x, y; t) = \int_{-\infty}^{+\infty} \int_{-\infty}^{+\infty} G_n(x, y, t|x_0, y_0, t_0 = 0) \frac{e^{-(x_0^2+y_0^2)/2\alpha^2}}{2\pi\alpha^2} dx_0 dy_0. \tag{63}$$

Substituting (56), and performing the x_0 and y_0 integrals, we find

$$a_n^+(x, y; t) = e^{-it} \frac{\exp\left(\frac{-(x^2 + y^2)}{2\alpha^2 + i2\varepsilon_n t}\right)}{2\pi(\alpha^2 + i\varepsilon_n t)}. \quad (64)$$

Note that as $t \downarrow 0$ the initial condition (62) is satisfied. At any time the amplitude of the field decays exponentially for large x, y and for any n the solution behaves well, i.e. it is finite everywhere. It is oscillatory with increasing distance $r = (x^2 + y^2)^{1/2}$ from the origin, and has a Gaussian envelope which spreads with increasing time while simultaneously decaying in amplitude. For each n the evolution is the same, only at different rates since time is scaled by ε_n . The fastest evolution is for the first baroclinic mode, and at large times and large horizontal distances this mode will eventually dominate. At intermediate times and distances usually many modes need to be summed in (58). In §4 we investigate how these various rates of horizontal dispersion for the various vertical modes combine in the case of constant N^2 , when the ϕ_n are trigonometric functions. The spectrum of the above initial condition is

$$\frac{1}{2\pi} \int_{-\infty}^{+\infty} \int_{-\infty}^{+\infty} a_n^+(x, y; t=0) e^{i(kx+ly)} dx dy = e^{-\alpha^2(k^2+l^2)/2},$$

and for any $\alpha > 0$ it decays exponentially for large horizontal wavenumbers.

In Appendix A we discuss an alternative to employing the Green's function for initial value problems. It involves expansions in time-dependent similarity solutions of the diffusion equation with complex time. Many exact solutions to initial value problems can be obtained with these expansions, like the dispersion of a one-dimensional storm track, as done numerically by Gill (1984), and numerous other interesting ones. Also various asymptotic results (large time limits) can be obtained, because the similarity solutions decay in amplitude at different rates.

4. Case of constant N^2

4.1. Poisson-converted series

The results of §3 and Appendix A are valid for any set of normal modes, i.e. for arbitrary $N^2(z)$ profiles. To obtain a picture of the evolution of a given initial condition, one needs to sum over the normal modes, which for most N^2 profiles will have to be done numerically. In the case of constant N^2 various other interesting results can be obtained which show how the different dispersion rates associated with the vertical modes combine. With N^2 constant the eigenfunctions $\phi_n(z)$ are given by (50) and the Rossby radii R_n by

$$R_n^2 = \frac{N^2}{f_0^2} \frac{H^2}{(n\pi)^2}. \quad (65)$$

The parameter ε_n appearing in (56) is in this case

$$\varepsilon_n = \frac{R_n^2}{L^2} = \frac{\varepsilon}{(n\pi)^2}, \quad (66)$$

with ε the Burger number, as in (44). Substitution in (56) shows that the Green's function is formally equal to

$$G(x, y, z, t | x_0, y_0, z_0, t_0) = \frac{U(t - t_0)e^{-i(t-t_0)}}{i\pi\varepsilon(t - t_0)} \sum_{n=1}^{\infty} (n\pi)^2 \exp\left(\frac{iR^2(n\pi)^2}{2\varepsilon(t - t_0)}\right) \cos(n\pi z_0) \cos(n\pi z), \tag{67}$$

with R as in (57). Owing to the factor $(n\pi)^2$ this series is divergent. Convergent expressions are found whenever the Green's function is convoluted with a finite-sized initial condition. If the resulting series is absolutely convergent, the Poisson sum formula can be applied. This converts the series expansion of normal modes into another one which has a simple interpretation. Consider the initial condition $a^+(x, y, z; t = 0) = \delta(x - x_0)\delta(y - y_0)f(z)$, with $\int_{-1}^0 f(z)dz = 0$. If we call $f_n = \int_{-1}^0 f(z_0)\phi_n(z_0)dz_0$, then the evolution is for $t > 0$

$$a^+(x, y, z; t) = \frac{e^{-it}}{i\pi\varepsilon t} \sum_{n=1}^{\infty} f_n(n\pi)^2 \exp\left(\frac{iR^2(n\pi)^2}{2\varepsilon t}\right) \cos(n\pi z). \tag{68}$$

We take for f a narrow Gaussian centred around $z = -d$, with $d \in (-1, 0)$:

$$f(z) = \frac{1}{(2\pi\alpha)^{1/2}} e^{-(z+d)^2/2\alpha^2} - 1.$$

If we choose α very small, we find that to a high degree of accuracy

$$f_n = \sqrt{2}e^{-(n\pi)^2\alpha^2/2} \cos(n\pi d).$$

Substitution in (68) yields

$$a^+(x, y, z; t) = \frac{\sqrt{2}e^{-it}}{i\pi\varepsilon t} \frac{\partial^2}{\partial z^2} S,$$

with

$$S = \sum_{n=1}^{\infty} \exp\left(\frac{iR^2(n\pi)^2}{2\varepsilon t} - \frac{(n\pi)^2\alpha^2}{2}\right) \cos(n\pi d) \cos(n\pi z).$$

We observe that S is a sum of type $\sum f(n\pi)$. The Poisson sum formula tells that this sum is equal to (Carrier, Krook & Pearson 1966)

$$S = \sum_{n=1}^{\infty} f(n\pi) = \left(\frac{2}{\pi}\right)^{1/2} \left(\frac{1}{2}F_c(0) + \sum_{p=1}^{\infty} F_c(2p)\right) - \frac{1}{2}f(0),$$

$$F_c(p) = \left(\frac{2}{\pi}\right)^{1/2} \int_0^{\infty} \cos(pm)f(m)dm. \tag{69}$$

Applying the Poisson sum formula to S , we find with some elementary integrations

$$a^+(x, y, z; t > 0) = \sum_{p=-\infty}^{+\infty} G(z + d - 2p) + G(z - d - 2p), \tag{70}$$

where

$$G(z) = \frac{e^{-it}}{(2\pi)^{3/2}} \left[\frac{(\varepsilon t)^{1/2}}{(iR^2 - \alpha^2\varepsilon t)^{3/2}} + \frac{(\varepsilon t)^{3/2}z^2}{(iR^2 - \alpha^2\varepsilon t)^{5/2}} \right] \exp\left(\frac{\frac{1}{2}z^2\varepsilon t}{iR^2 - \alpha^2\varepsilon t}\right). \tag{71}$$

R is again as in (57). By direct integration of (71) it is found that for any $\Delta x, \Delta y$ one has

$$\lim_{t \downarrow 0} \int_{x_0 - \Delta x}^{x_0 + \Delta x} \int_{y_0 - \Delta y}^{y_0 + \Delta y} G dx dy = \frac{e^{-z^2/2\alpha^2}}{(2\pi)^{1/2}\alpha},$$

and it appears that $G(z)$ is the evolution of the initial condition $\delta(x)\delta(y)\delta(z)$ on the infinite domain, with $\delta(z)$ approximated by the Gaussian bump (α arbitrarily small). This cannot be inferred from a consideration of (29) because the definition of the integral operator \mathcal{L} cannot be extended to the infinite interval. It can, however, be shown by a consideration of the differential version (36) for the infinite domain. The eigenfunctions of the $(d/dz)^2$ operator are $\exp(imz)$ for any m , and one can solve the initial value problem with, for instance, a Fourier-transform method.

The wavy part of (71) is determined by the factor in the exponential. The term in the square bracket is important for the amplitude of the wavefield but not for the oscillation frequency (this is easily seen by writing each term as $A(R, z, t) \exp(i\theta(R, z, t))$, with A real). For very small α at given z, R the oscillation frequency for $t \ll R^2/\varepsilon\alpha^2$ is to a good approximation

$$\omega(R, z) = 1 + \frac{1}{2}\varepsilon \frac{z^2}{R^2}. \tag{72}$$

This can be explained by a consideration of the dispersion relation. For a plane wave $e^{i(kx+ly+mz-\omega t)}$ we have (substitute in non-dimensionalized (17))

$$\omega = 1 + \frac{1}{2}\varepsilon \frac{k^2 + l^2}{m^2}.$$

The three-dimensional group velocity vector has the components

$$c_g = \left(\frac{\partial \omega}{\partial k}, \frac{\partial \omega}{\partial l}, \frac{\partial \omega}{\partial m} \right) = \varepsilon \left(\frac{k}{m^2}, \frac{l}{m^2}, \frac{-(k^2 + l^2)}{m^3} \right) \tag{73}$$

and is perpendicular to the wavevector with components k, l, m . So if an observer is at position R, z with respect to a source, which consists of a combination of all possible plane waves, he/she will only see waves come by which satisfy $|m|/(k^2 + l^2)^{1/2} = R/|z|$, or in other words, waves with the frequency given by (72).

The solution on the infinite domain (71) can be written as a similarity solution

$$\left. \begin{aligned} G(z) &= \frac{e^{-it}}{\alpha^3 \varepsilon t (2\pi)^{3/2}} \left[\frac{1}{(iR'^2 - 1)^{3/2}} + \frac{z'^2}{(iR'^2 - 1)^{5/2}} \right] \exp\left(\frac{\frac{1}{2}z'^2}{iR'^2 - 1}\right), \\ R' &= \frac{R}{\alpha(\varepsilon t)^{1/2}}, \quad z' = \frac{z}{\alpha}. \end{aligned} \right\} \tag{74}$$

Thus, as time increases the amplitude decreases uniformly with t^{-1} while a simultaneous stretching in the radial direction occurs, while for smaller α the amplitude of G increases uniformly while there is further compression uniformly in both the horizontal and the vertical direction. In figure 2 where we show contours of $\alpha^3 \varepsilon t |G|$ as a function of R' and z' . The largest amplitude at any time is at $z' = R' = 0$ and it decays rapidly with increasing $|z'|$. At any given time the response goes to zero as distance to the source point goes to infinity. At early times large-amplitude high-frequency waves propagate from the source mainly in the vertical direction, while at later times the propagation direction gets an increasingly larger horizontal component, with lower-frequency waves.

In (70) the G are distributed throughout infinite space such that at $z = -1, 0$ the

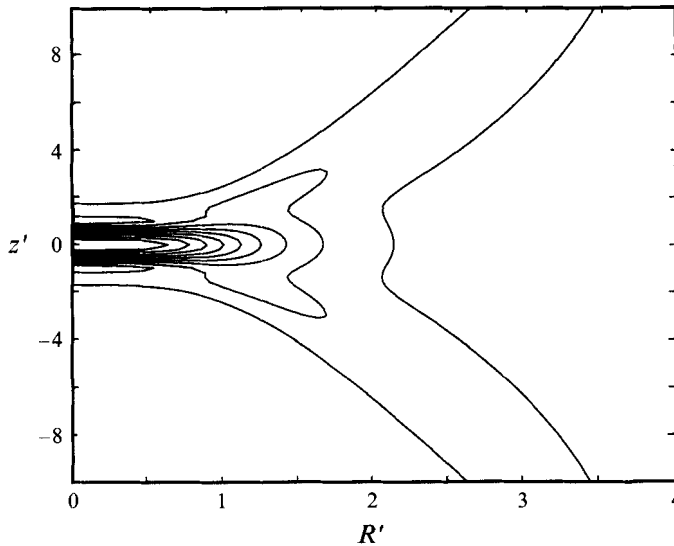


FIGURE 2. Contours of $\alpha^3 et|G|$ as a function of the scaled vertical distance z' and scaled horizontal distance R' , as given by (74). G gives the evolution of the initial condition $\delta(x)\delta(y)\delta(z)$ with $\delta(z)$ approximated by a Gaussian bump $((2\pi)^{1/2}\alpha)^{-1} \exp(-z^2/2\alpha^2)$. Contour increments are $1/10$ of the maximum at $R' = z' = 0$.

boundary conditions are satisfied, i.e. $\partial_z a^+ = 0$. When (67) is considered to apply to all z , it describes the evolution of the initial condition

$$a^+(x, y, z; t = t_0) = \delta(x - x_0)\delta(y - y_0) \left(\sum_{p=-\infty}^{+\infty} [\delta(z + d - 2p) + \delta(z - d - 2p)] - 1 \right)$$

on the infinite domain. The solution for the finite domain (70) is analogous to that found in electrostatics problems, where boundary conditions on parallel plates for the field due a charge are satisfied by first considering the solution on the infinite domain, and then by adding strategically located ‘image charges’. In our problem, the boundary condition $\partial_z a^+ = 0$ was derived from the no-flux condition on the vertical component w of the velocity field. On a semi-infinite vertical domain with boundary condition $w = 0$ at, say, $z = 0$, the evolution of a narrow Gaussian bump at $z = -d$ would be $G(z + d) + G(z - d)$, the first term being the response on the infinite domain, the second an ‘image’ at $z = +d$. By symmetry the addition of the second term makes $w = 0$ at $z = 0$. Then, to satisfy also the boundary condition $w = 0$ at $z = -1$, an infinite number of image points needs to be added, leading to (70). If one has small wavepackets in mind, the image points can also be interpreted as describing the various reflections at the upper and lower boundary. To get an accurate picture of the response in the finite vertical domain, few of the image points are needed because they are at increasing vertical distances away (increasing p in (70)) and the amplitude of G decays exponentially with $|z|$. At any given time fewer image points are needed at small R than at larger R .

Consider now the case where the initial condition is of the form

$$a^+(x, y, z; t = 0) = [\delta(z - z_0) - 1]e^{-r^2/2}, \quad r^2 = x^2 + y^2 \tag{75}$$

where $z_0 \in (-1, 0)$. This is the converse of the previous example, i.e. this initial condition has finite horizontal size, combined with a δ -structure in the vertical. The solution with (75) as initial condition will be denoted by $a_\delta^+(x, y, z; t|z_0)$. Projection

on the n th mode gives

$$a_n^+(x, y; t = 0) = e^{-r^2/2} \phi_n(z_0). \quad (76)$$

With (59) the evolution of (76) is the same as the example given in §3.3 (see expression (64) with $\alpha = 1$ and without the factor 2π). Using the definition of ε_n (66), we find with (58)

$$\begin{aligned} a_\delta^+(x, y, z; t|z_0) &= e^{-it} \left[\sum_{n=1}^{\infty} \frac{2(n\pi)^2}{(n\pi)^2 + i\epsilon t} \exp\left(\frac{-(n\pi)^2 r^2/2}{(n\pi)^2 + i\epsilon t}\right) \cos(n\pi z_0) \cos(n\pi z) \right] \\ &\equiv \frac{\partial^2 A_\delta^+(x, y, z; t|z_0)}{\partial z_0^2}. \end{aligned} \quad (77)$$

In Appendix B we show through an application of the Poisson sum formula that

$$\begin{aligned} A_\delta^+(x, y, z; t|z_0) &= \frac{-e^{-it-r^2/2}}{ia(t)} \left\{ \sum_{p=-\infty}^{\infty} e^{ia(t)|z \pm z_0 - 2p|} \int_0^{\infty} J_0(r(ia(t)|z \pm z_0 - 2p| - x)^{1/2}) I_0(rx^{1/2}) e^{-2x} dx \right\}. \end{aligned} \quad (78)$$

Note that this is a sum similar to (70). The J_0, I_0 are zeroth-order Bessel functions (Watson 1966). The time-dependent factor $ia(t)$ is

$$ia(t) = -e^{i\pi/4} (\epsilon t)^{1/2} = -(\epsilon t/2)^{1/2} - i(\epsilon t/2)^{1/2}, \quad (79)$$

so for $t > 0$ the amplitudes of the terms $e^{ia(t)|z \pm d - 2p|}$ decay exponentially, both with increasing time and increasing p . This implies that, again, as time progresses less and less terms are needed, i.e. the contribution from terms with large p (distant ‘image points’) become negligible.

4.2. Example of three-dimensional evolution

Solution (77) remains singular (infinite amplitude) at $z = z_0$ at all times. This singular behaviour disappears when we also give the initial condition some finite vertical structure. For instance, consider

$$a^+(x, y, z; t = 0) = e^{-r^2/2} f(z), \quad (80)$$

with an $f(z)$ that has zero vertical average. a_δ^+ as given by (77) can be used as a Green’s function for initial conditions like this, and the evolution is

$$a^+(x, y, z; t) = \int_{-1}^0 f(z_0) a_\delta^+(x, y, z; t|z_0) dz_0. \quad (81)$$

As an example we take the case where

$$\begin{aligned} f(z) &= -1, \quad -1 \leq z < -d \\ &= \frac{1-d}{d}, \quad -d < z \leq 0. \end{aligned} \quad (82)$$

Since to lowest order in the Burger number $a^+ = u + iv$ this is an initial condition where the velocity field at any z is pointing along the x -direction, with a Gaussian amplitude distribution. For small d it has a large positive amplitude in a narrow region just underneath the upper surface. This is a realistic z -dependent amplitude

for cases where an impulsive force is applied at the upper surface, and the barotropic (vertically averaged) response has been subtracted. According to (81) the evolution is

$$\begin{aligned}
 a^+(x, y, z; t) &= \int_{-1}^0 f(z_0) \frac{\partial^2 A_\delta^+(x, y, z; t|z_0)}{\partial z_0^2} dz_0 \\
 &= - \int_{-1}^{-d} \frac{\partial^2 A_\delta^+}{\partial z_0^2} dz_0 + \frac{1-d}{d} \int_{-d}^0 \frac{\partial^2 A_\delta^+}{\partial z_0^2} dz_0 = \frac{-1}{d} \frac{\partial A_\delta^+}{\partial z_0} \Big|_{z_0=-d}, \quad (83)
 \end{aligned}$$

where we have used that the derivative of A_δ^+ vanishes at the bottom and at the surface (this follows from (77)). Other $f(z)$ with more steps, or piecewise linear, can be handled with equal ease as (82).

Whenever we differentiate functions of type $g(|z_0 + b|)$ (as are the terms appearing in (78)), we have

$$\frac{dg(|\pm z_0 + b|)}{dz_0} = \text{sgn}(\pm z_0) \text{sgn}(\pm z_0 + b) g'$$

(a prime denotes differentiation), where $\text{sgn}(x) = -1 + 2U(x)$, with U again the Heaviside function. Using this we find

$$\begin{aligned}
 a^+(x, y, z; t) &= \frac{-e^{-it - \frac{1}{2}r^2}}{d} \sum_{p=-\infty}^{\infty} \text{sgn}(\pm d) \text{sgn}(z \pm d - 2p) e^{ia(t)|z \pm d - 2p|} \\
 &\quad \times \int_0^\infty J_0(\dots) I_0(rx^{1/2}) e^{-2x} dx \\
 &\quad + \frac{r^2 e^{-it - r^2/2}}{2d} \sum_{p=-\infty}^{\infty} \text{sgn}(\pm d) \text{sgn}(z \pm d - 2p) e^{ia(t)|z \pm d - 2p|} \\
 &\quad \int_0^\infty \frac{J_1(\dots)}{(\dots)} I_0(rx^{1/2}) e^{-2x} dx, \quad (84)
 \end{aligned}$$

where terms (\dots) are as in (78) with $z_0 = -d$ and with the combination of $z \pm d - 2p$ the same as in the exponential they are multiplied by. To arrive at this form we have used the identity (see Watson 1966) $J_0'(z) = -J_1(z)$. With (84) we can determine the evolution at $r = 0$. In the limit $r \rightarrow 0$, the terms containing $J_1(\dots)/(\dots)$ tend to a finite value, and the parts of (84) that are multiplied by r^2 are thus zero. Furthermore, since $J_0(0) = I_0(0) = 1$, at $r = 0$ we have $\int_0^\infty J_0(0) I_0(0) e^{-2x} dx = -1/2$, and the evolution at $r = 0$ is

$$a^+ = \frac{e^{-it}}{2d} \sum_{p=-\infty}^{\infty} \text{sgn}(\pm d) \text{sgn}(z \pm d - 2p) e^{ia(t)|z \pm d - 2p|}. \quad (85)$$

With (85) and (79) we find that for $t \rightarrow \infty$ the solution goes to zero everywhere except at the point $z = -d$. On one side $z = -d^+$ (i.e. approaching $z = -d$ from above in the upper layer) it goes to $(2d)^{-1}$, on the other side $z = -d^-$ (in the lower layer) it goes to $-(2d)^{-1}$, i.e. there is a phase jump of 180° . The amplitude which is initially discontinuous becomes asymptotically continuous. Near the step location energy in the upper layer is decreasing while it increases near $z = -d$ in the lower layer. For all $z \neq -d$ every term tends to zero for increasing time, and for large time all the energy will get concentrated in a narrow layer around $z = -d$. This is illustrated in figure 3 where we have plotted the amplitude at $r = 0$ at several times. The dashed line indicates the initial amplitude, in this case for $d = 0.2$, and the solid lines the amplitude at several later times, as indicated. At $et = 1$ (for a Burger number $\epsilon = 0.1$

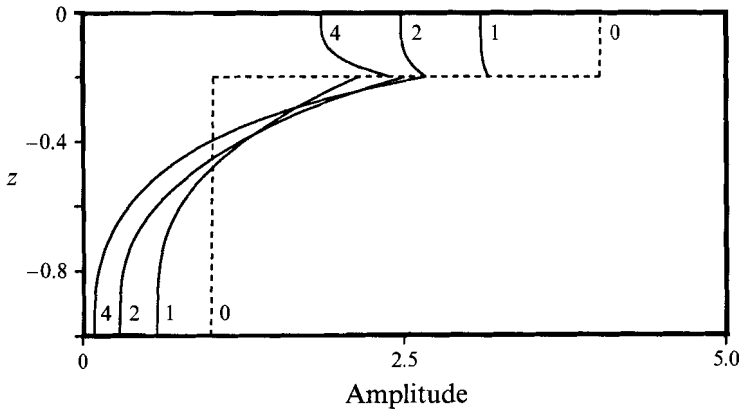


FIGURE 3. Graph showing the amplitude evolution of the Gaussian (80) with an initial baroclinic step (82) of thickness $d = 0.2$ at $r = 0$ as a function of depth according to (85). The initial amplitude is shown as a dashed line while the solid lines indicate the amplitude at times $et = 1, 2$ and 4 . For large time the amplitude is approximately $(2d)^{-1} \exp(-(et/2)^{1/2}|z + d|)$ when the step is at $z = -d$.

this is after 10 inertial periods) the amplitude has decreased in the upper layer as well as in the lower half of the lower layer (i.e. between approximately $-1 \leq z < 0.5$). In the upper region of the lower layer the amplitude has increased. At later times, $et = 2, 4$, we see that in the upper layer near the surface the amplitude continues to decrease but it tends to a value $2.5 (= (2d)^{-1})$ near $z = -d$. Similarly in the upper part of the lower layer near $z = -d$ the amplitude keeps increasing to a value of $(2d)^{-1}$ but in the lower part it goes to zero. Already for $et = 1$ few ‘image points’ (the terms containing $p = 1, 2, \dots$) are needed to obtain a fractional accuracy of 10^{-3} . Note that at all times shown in figure 3 the vertical derivatives are zero at the surface and the bottom, which indicates that enough ‘image points’ have been used.

For $r \neq 0$ the integrals involving the products of Bessel functions in (84) cannot be evaluated in closed form. A numerical program was written which evaluated the integrals, and summed over the image sources until a fractional accuracy of 10^{-3} at each point was obtained. In order to evaluate the integrals over the infinite line, we only integrated to a certain x_{\max} , such that beyond this point the integrands were negligibly small. These integrals were calculated using eighth-order Romberg integration, with a trapezoidal rule, and extrapolation to zero step size by means of rational function extrapolation of the Bulirsch–Stoer type (see Press *et al.*, 1990). The Bessel functions of complex argument were obtained from the commercially available IMSL numerical package.

We find that for small r the amplitude evolution is similar to that shown in figure 3 for $r = 0$ while for large r the amplitude is proportional to that of the first baroclinic mode, which has the fastest horizontal dispersion rate. A qualitative overview of the evolution is obtained by plotting the contours of constant amplitude at various times. In figure 4 we plot the evolution between $et = 0$ (the initial condition) and $et = 1$ for the case $d = 0.2$. In figure 4(a) we show the initial condition (80) with f given by (82). The straight lines below the step position correspond to the fact that the amplitude is there depth independent and equal to $\exp(-r^2/2)$. In the upper layer the amplitude is $\exp(-r^2/2)(1 - d)/d$, which is much larger at the same r position. The contour plotting software has some problems around the step position, because of this discontinuity, and the lines are for that reason bent a little. In parts (b–f)

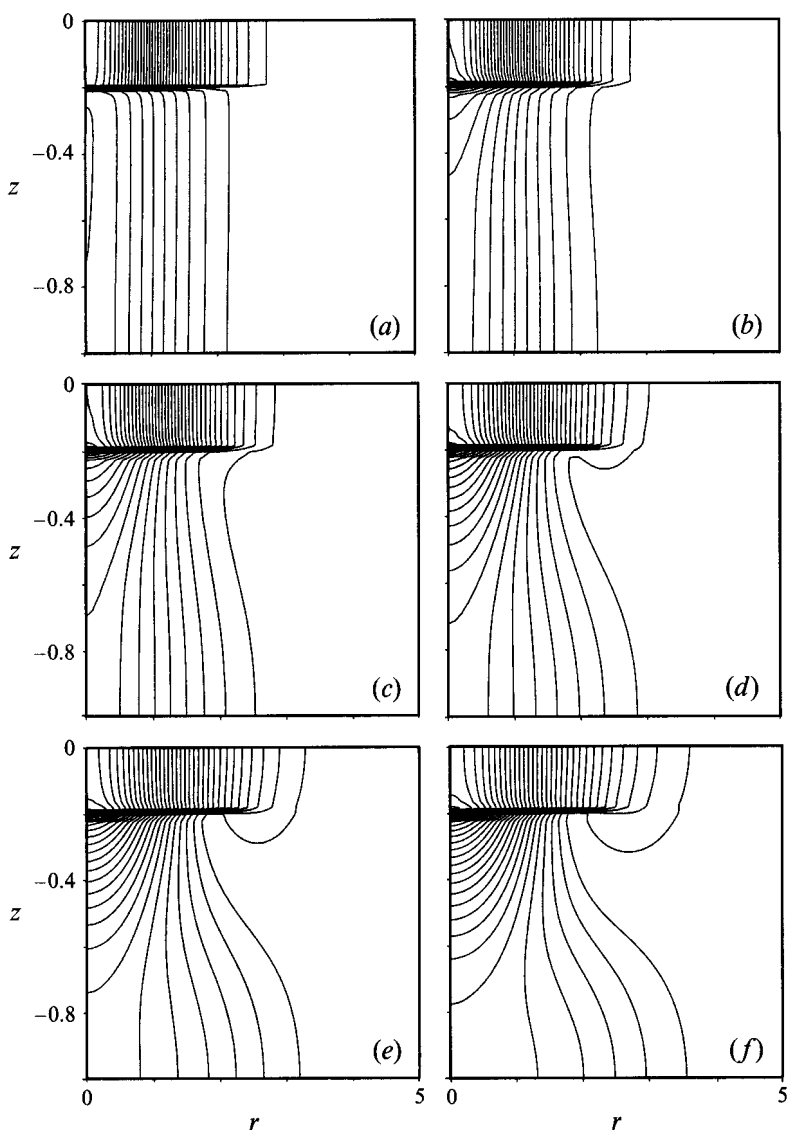


FIGURE 4. Graphs showing the evolution of the Gaussian (80) with an initial baroclinic step (82) of thickness $d = 0.2$. Contours of constant amplitude are shown here. Times are (a) $et = 0$ (initial condition), (b) $et = 0.2$, (c) $et = 0.4$, (d) $et = 0.6$, (e) $et = 0.8$, and (f) $et = 1.0$. Contour increments are 0.1.

snapshots of the field are shown in time steps of $\Delta et = 0.2$. The outermost contour has a value of 0.1 here, and is seen to propagate outwards near the bottom and the surface. A typical bulging pattern evolves at the outer side of the Gaussian near the surface. Near the step at $r = 2$ we see that at $et = 1.0$ (figure 4f) energy has decreased. Note that near the surface the discontinuity can be seen to propagate.

In figure 5 we 'zoom out', and continue from $et = 1$ to $et = 4$. The contour with value 0.1 has at $et = 4$ (figure 5d) moved far to the right, while the piling up of energy near the core below the step is clearly visible. A secondary maximum develops at the bottom but with low amplitude. The pattern thus established persists at even later times (not shown), while shifting further to the right. When we look at the far

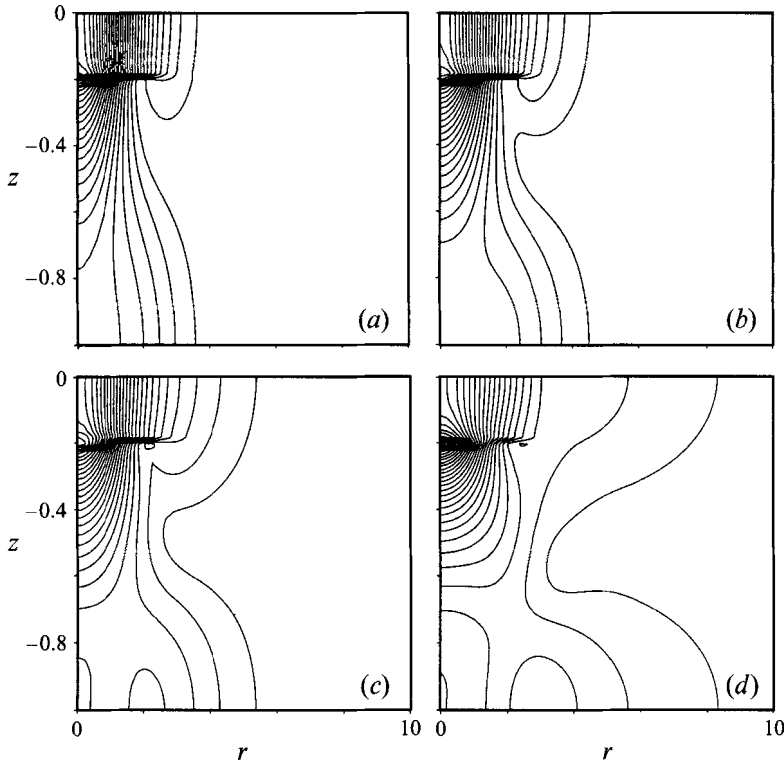


FIGURE 5. Continuation of figure 4 plotted on a wider horizontal scale. Times are (a) $et = 1.0$ (as figure 4f) (b) $et = 1.5$, (c) $et = 2.0$, and (d) $et = 4.0$. Contour increments are 0.1.

field in more detail we find that the amplitude at large time is dominated by the first baroclinic mode, as expected from the dispersion relation. There the normal modes sum is more efficient than our Poisson converted series.

In §2 we showed that in the unforced case energy has to be conserved. Although amplitudes grow at larger r , they remain small compared to the initial amplitudes near the centre of the Gaussian. We have checked our solutions for energy conservation. The total energy corresponding to the plots shown in figure 4 and figure 5 was found to vary less than 0.1% in a time interval $et = 4$. In polar coordinates the energy integral is $\frac{1}{2} \int \int |a^+|^2 r dr d\theta$, and the factor r weights the contribution at larger r in favour of those at small r , i.e. there is geometrical attenuation.

After a time interval $et = 4$ we find that the frequencies are everywhere very close to the Coriolis frequency if ε is small. Only in the very early stages are appreciably super-inertial frequencies observed. For instance after 10 inertial periods frequencies of about $1.03f_0$ are found near the bottom when $\varepsilon = 0.1$. For higher Burger numbers, the frequencies are higher, and vice versa closer to f_0 when the Burger number is smaller. In the early stages we find that the frequencies increase monotonically with depth for all r .

Finally we remark that a sufficiently large sum of normal modes converges to the solutions like shown in figures 4 and 5. With 200 normal modes summed there is essentially no difference in all these cases. For large time and large r it is actually computationally advantageous to use a normal modes sum, since the integration over Bessel functions involves large arguments of the Bessel functions, and there are

limitations on how large these can be in numerical packages like IMSL which we used. For r not too large and large time the Poisson converted series is very effective because few 'images' are needed, and the integrals involving the Bessel functions converge rapidly.

5. Summary and discussion

We have investigated the evolution of near-inertial internal waves in horizontal-vertical space. We assumed the Burger number to be small and considered baroclinic waves in a layer of constant depth. The equations of motion can be formulated either in integral or in differential form. In the main body of the paper we work with the integral formulation, which is first order in time. First we formulated the Green's function formula for the problem, taking into account that our equations govern baroclinic disturbances only. For depth-dependent Brunt-Väisälä frequency a normal modes expansion is employed. The Green's function is very singular. This is due to the long-wave approximation (small Burger number limit) which allows for unbounded horizontal group velocity for waves with very large horizontal wavenumbers. Well-behaved solutions are found when convoluted with an initial condition that has vanishing energy in the large horizontal wavenumbers. The evolution of a given initial condition projected on a vertical normal mode can analytically be determined with expansions in similarity solutions. This is an alternative to using the Green's function. Based on this observation many interesting exact solutions can be constructed which would be hard otherwise. Each vertical normal mode has a distinct horizontal dispersion rate which is fastest for the first baroclinic mode, which therefore appears first at large distances from some localized source. For non-constant Brunt-Väisälä frequency all one can do is sum over normal modes, and how the various different dispersion rates combine can only be determined numerically. For constant buoyancy frequency we find that the normal modes series can be converted into another series by application of the Poisson sum formula. This new series can also be obtained by applying the method of images, starting from the differential formulation on an infinite layer. At present it is not clear whether the method of images can also be applied to non-constant N^2 -profiles and what its relation is to the normal modes expansion. The conversion by means of the Poisson sum formula is very effective in that the resulting series converge rapidly. We first showed that for a highly concentrated initial condition the entire field can be expressed (to a high degree of accuracy) with just a few analytical expressions in closed form which bring out the z , R and time dependence in a clear fashion (R being the horizontal distance to the source point and z the vertical distance). The normal modes sum does not yield any clues concerning the overall behaviour thus obtained. The lowest-order term in the Poisson-converted expansion corresponds to the response on the infinite domain. Close to either the surface or the bottom, image sources are needed to satisfy the boundary conditions. These image sources can be thought of as representing the reflections of the waves at the upper and lower boundary, where the no-flux condition is prescribed (the free surface is replaced by a rigid lid, which eliminates the barotropic part from the problem). Finally, we considered the evolution of an initial condition which has an isotropic Gaussian amplitude distribution in the horizontal and which is confined to a narrow layer at the upper surface. Again a Poisson-converted series is used which is very effective for large times and not too large horizontal distances from the centre of the Gaussian. The evolution of the initial condition shows the following features:

(i) The timescale of the evolution of the amplitude is determined by the value of the Burger number ε .

(ii) The energy propagates radially outwards. Near the center of the Gaussian the energy decreases both in the surface layer and near the bottom but increases underneath the step.

(iii) At large times and radial distances the amplitude and phase fields become dominated by the first baroclinic mode.

(iv) In the intermediate time and space ranges the amplitude slowly penetrates into the interior and outward in a bulging way. No simple normal-mode-related interpretation is possible for this phase of the evolution.

Further detailed analysis of this particular case shows that no significant scale separation develops between the wavefield and the amplitude envelope and that the evolution in the lower layer is insensitive to the exact step thickness as long as it is small compared to the total layer depth.

Appendix A. Expansions in similarity solutions

Here we show that there is an alternative to using the Green's function for initial value problems as discussed in §3. By putting $a_n^+ = e^{-it}a_n(x, y; t)$ in (61) this is transformed into

$$\partial_t a_n - i\frac{1}{2}\varepsilon_n \nabla_h^2 a_n = 0. \quad (\text{A } 1)$$

If we define a complex time variable $\tilde{t} = i\frac{1}{2}\varepsilon_n t$, we get the two-dimensional diffusion equation

$$\partial_{\tilde{t}} a_n = \nabla_h^2 a_n. \quad (\text{A } 2)$$

For *real* \tilde{t} a well-known exact solution to (A 2) is

$$a_n(x, y; \tilde{t}) = \frac{\exp(-(x^2 + y^2)/(2\alpha^2 + 4\tilde{t}))}{2\pi(\alpha^2 + 2\tilde{t})}.$$

In the limit $\alpha \downarrow 0$ this is the Green's function for the diffusion equation (Morse & Feshbach 1953). If we substitute for the complex time and multiply by e^{-it} , we get the a_n^+ found in §3.3 (see (64)) through use of the Green's function.

For the two-dimensional diffusion equation (A 2) we can use the results of Kloosterziel (1990) and substitute for complex time. In that paper the following results were established. Assume that an initial condition for (A 2) satisfies (we drop the tilde on t for convenience)

$$\iint |a_n(x, y; t = 0)|^2 e^{(x^2 + y^2)/2} dx dy < \infty.$$

For rectangular coordinates one can then write

$$a_n(x, y; t = 0) = \sum_{l=0}^{\infty} \sum_{m=0}^{\infty} a_{lm} \Omega_l(x) \Omega_m(y), \quad (\text{A } 3)$$

where the Ω are given by

$$\Omega_n(x) = \frac{H_n(x/\sqrt{2}) e^{-x^2/2}}{(2^n n! (2\pi)^{1/2})^{1/2}}, \quad H_n(x) = (-1)^n e^{x^2} \frac{d^n}{dx^n} e^{-x^2} \quad (n = 0, 1, 2, \dots). \quad (\text{A } 4)$$

Here H_n is a Hermite polynomial of degree n . The functions Ω_i are orthonormal with

respect to the weight function $\exp(x^2/2)$, i.e.

$$\int_{-\infty}^{+\infty} \Omega_l(x)\Omega_m(x)e^{x^2/2}dx = \delta_{lm}.$$

The expansion coefficients a_{lm} in (A 3) are calculated according to

$$a_{lm} = \int_{-\infty}^{+\infty} \int_{-\infty}^{+\infty} a_n(x, y; t = 0)\Omega_l(x)\Omega_m(y)e^{(x^2+y^2)/2}dx dy. \tag{A 5}$$

It is shown in Kloosterziel (1990) that each Ω_l provides an exact *similarity* solution of the diffusion equation (A 2), i.e. when $\Omega_l(x)$ is an initial condition to (A 2) then the evolution is given by

$$a_n(x; t) = \frac{1}{b(t)^{l+1}}\Omega_l(x/b(t)), \quad b(t) = (2t + 1)^{1/2}. \tag{A 6}$$

In general, when an initial condition is given by (A 3), the evolution is given by

$$a_n(x, y; t) = \sum_{l=0}^{\infty} \sum_{m=0}^{\infty} \frac{a_{lm}}{b(t)^{2+l+m}}\Omega_l(x/b(t))\Omega_m(y/b(t)). \tag{A 7}$$

An alternative is to employ polar coordinates. We can expand as follows:

$$a_n(r, \theta; t = 0) = \sum_{m=0}^{\infty} \sum_{k=-m}^{k=+m} a_{mk}\Phi_{mk}(r, \theta), \tag{A 8}$$

where

$$\Phi_{mk}(r, \theta) = \left(\frac{(m - |k|)!}{2\pi(m!)^3}\right)^{1/2} (r^2/2)^{|k|/2}e^{-r^2/2}L_m^{|k|}(r^2/2)e^{ik\theta}. \tag{A 9}$$

Here L_m^n is an associated Laguerre polynomial defined by

$$L_m^n(y) = \frac{d^n L_m(y)}{dy^n}, \quad L_m(y) = e^y \frac{d^m}{dy^m} y^m e^{-y} \quad (m = 0, 1, 2, \dots). \tag{A 10}$$

The Φ_{mk} form a complete orthonormal set in the Hilbert space $L_2(\mathbf{R}^2, e^{r^2/2})$, and satisfy

$$\int_0^{\infty} \int_0^{2\pi} \Phi_{mk}\Phi_{m'k'}^* e^{r^2/2} r d\theta dr = \delta_{mm'}\delta_{kk'}.$$

A * here denotes complex conjugate. The expansion coefficients (which are complex) are calculated according to

$$a_{mk} = \int_0^{\infty} \int_0^{2\pi} a_n(r, \theta; t = 0)\Phi_{mk}^*(r, \theta)e^{r^2/2} r d\theta dr. \tag{A 11}$$

Each of these Φ is again an exact similarity solution of the diffusion equation, that is, if a Φ_{mk} is provided as initial condition, then at later times the solution is

$$a_n(r, \theta; t) = \frac{1}{b(t)^{2m+2-|k|}}\Phi_{mk}(r/(b(t), \theta),$$

where $b(t)$ is as in (A 6). Therefore, if an initial condition can be written as (A 8) (that is, if the initial condition is square-integrable with respect to the exponentially

growing weight function), the evolution is

$$a_n(r, \theta; t) = \sum_{m=0}^{\infty} \sum_{k=-m}^{k=+m} \frac{a_{mk}}{b(t)^{2m+2-|k|}} \Phi_{mk}(r/(b(t), \theta)). \tag{A 12}$$

All these functions are analytic in t however, so this result also applies to (A 1), and all one needs to do is to replace the real time in the above expressions by purely imaginary time. The recipe is thus: project an initial condition on mode n to obtain $a_n(x, y; t = 0)$. Expand a_n in similarity solutions and substitute $t = i\frac{1}{2}\varepsilon_n t$. Then, a sum over all normal modes and multiplication by e^{-it} gives the full evolution.

Appendix B. Evaluation of Poisson sum formula

First we write the sum in the square brackets in (77) as

$$\sum_{n=1}^{\infty} (\dots) = -\frac{\partial^2}{\partial z_0^2} \sum_{n=1}^{\infty} \frac{2}{(n\pi)^2 + i\epsilon t} \exp\left(\frac{-(n\pi)^2 r^2/2}{(n\pi)^2 + i\epsilon t}\right) \cos(n\pi z_0) \cos(n\pi z). \tag{B 1}$$

For $t > 0$ we write

$$\frac{1}{(n\pi)^2 + i\epsilon t} = \frac{1}{(n\pi - a)(n\pi + a)}, \quad \frac{(n\pi)^2}{(n\pi)^2 + i\epsilon t} = 1 + \frac{a/2}{n\pi - a} - \frac{a/2}{n\pi + a},$$

where

$$a = i\epsilon^{1/4}(\epsilon t)^{1/2}. \tag{B 2}$$

With this substituted, the sum (B 1) is equal to

$$e^{-r^2/2} \sum_{n=1}^{\infty} f(n\pi)g(n\pi), \tag{B 3}$$

with

$$f(n) = \frac{\frac{1}{2}\sqrt{2}}{n-a} \exp\left(\frac{-r^2 a/4}{n-a}\right) (e^{inz_0} + e^{-inz_0}), \quad g(n) = \frac{\frac{1}{2}\sqrt{2}}{n+a} \exp\left(\frac{r^2 a/4}{n+a}\right) (e^{inz} + e^{-inz}). \tag{B 4}$$

Next, we apply (69). We note that the cosine transform of the product fg is

$$F_c(p) = \left(\frac{2}{\pi}\right)^{1/2} \int_0^{\infty} f(m)g(m) \cos(pm) dm = \frac{1}{2(2\pi)^{1/2}} \int_{-\infty}^{+\infty} f(m)g(m)(e^{ipm} + e^{-ipm}) dm$$

(because $f(-m)g(-m) = f(m)g(m)$). With the convolution theorem for Fourier-transforms (see Morse & Feshbach 1953) we have

$$F_c(p) = \frac{1}{2(2\pi)^{1/2}} \int_{-\infty}^{+\infty} F^+(l)G^+(p-l) dl + \frac{1}{2(2\pi)^{1/2}} \int_{-\infty}^{+\infty} F^-(l)G^-(p-l) dl, \tag{B 5}$$

where

$$F^{\pm}(l) = \frac{1}{(2\pi)^{1/2}} \int_{-\infty}^{+\infty} f(m)e^{\pm ilm} dm, \quad G^{\pm}(l) = \frac{1}{(2\pi)^{1/2}} \int_{-\infty}^{+\infty} g(m)e^{\pm ilm} dm.$$

With (B 4) these are

$$F^{\pm}(l) = \frac{\frac{1}{2}\sqrt{2}}{(2\pi)^{1/2}} \int_{-\infty}^{+\infty} \frac{\exp\left(\frac{(-r^2 a/4)/(m-a)}{m-a}\right) \{e^{im(z_0 \pm l)} + e^{im(-z_0 \pm l)}\} dm, \tag{B 6}$$

$$G^\pm(l) = \frac{\frac{1}{2}\sqrt{2}}{(2\pi)^{1/2}} \int_{-\infty}^{+\infty} \frac{\exp((r^2 a/4)/(m+a))}{m+a} \{e^{im(z\pm l)} + e^{im(-z\pm l)}\} dm. \quad (B7)$$

Owing to the factors $(m \pm a)^{-1}$, the integrands vanish for $m \rightarrow \pm\infty$. Thus, whenever for instance in F^\pm terms $\pm z_0 \pm l > 0$, we can close the contour in the upper half-plane, while when they are negative, we can close in the lower half-plane. For F^\pm there is an essential singularity at $m = a$, which is in the upper half-plane. For $\pm z_0 + l < 0$ we close in the lower half, and the result is zero. When either of these is > 0 we enclose the singularity in the upper half, and go around it in positive direction (anti-clockwise). Expanding

$$\exp\left(\frac{-r^2 a/4}{m-a}\right) = \sum_{n=0}^{\infty} \frac{1}{n!} \frac{(-r^2 a/4)^n}{(m-a)^n},$$

and substituting this in (B 6), we find for the first part of F^+ the integral

$$\frac{\frac{1}{2}\sqrt{2}}{(2\pi)^{1/2}} \int_{-\infty}^{+\infty} \sum_{n=0}^{\infty} \frac{1}{n!} \frac{(-r^2 a/4)^n}{(m-a)^{n+1}} e^{im(z_0+l)} dm.$$

Thus, for $z_0 + l > 0$ when we enclose the singularity at $m = a$ we get (dropping the numerical prefactor momentarily)

$$2\pi i \sum_{n=0}^{\infty} \frac{1}{n!n!} (-r^2 a/4)^n (i(z_0 + l))^n e^{ia(z_0+l)} = 2\pi i J_0(r(ia(z_0 + l))^{1/2}) e^{ia(z_0+l)},$$

where J_0 is the zeroth-order Bessel function (of complex argument). Introducing the Heaviside step function $U(x)$ again, we find

$$F^\pm(l) = i\pi^{1/2} [U(z_0 \pm l) J_0(r(ia(z_0 \pm l))^{1/2}) e^{ia(z_0 \pm l)} + U(-z_0 \pm l) J_0(r(ia(-z_0 \pm l))^{1/2}) e^{ia(-z_0 \pm l)}], \quad (B8)$$

and similarly

$$G^\pm(l) = i\pi^{1/2} [(U(z \pm l) - 1) J_0(r(-ia(z \pm l))^{1/2}) e^{-ia(z \pm l)} + (U(-z \pm l) - 1) J_0(r(-ia(-z \pm l))^{1/2}) e^{-ia(-z \pm l)}].$$

The Heaviside functions make the integration in (B 5) only start at such l that the terms $\pm z_0 \pm l$ occurring in $F^\pm(l)$ are positive, while the terms $\pm z \pm (p-l)$ in $G^\pm(p-l)$ are negative. With some effort one finds that for instance the cross-product in the convolution integral containing $U(z_0+l)(U(z+p-l)-1)$ leads to an integral of type

$$e^{ia|z+z_0+p|} \int_0^\infty J_0(r(ia|z+z_0+p|+ias)^{1/2}) J_0(r(ias)^{1/2}) e^{2ias} ds.$$

Keeping carefully track of signs and numerical prefactors we find

$$F_c(2p) = -\frac{1}{2} \left(\frac{\pi}{2}\right)^{1/2} \sum e^{ia|\pm z \pm z_0 \pm 2p|} \int_0^\infty J_0(r(ia|\pm z \pm z_0 \pm 2p|+ias)^{1/2}) J_0(r(ias)^{1/2}) e^{2ias} ds, \quad (B9)$$

where the sum is over all eight combinations of $\pm z \pm z_0 \pm 2p$. Note that the term containing, say, $z + z_0 - 2p$ is equal to the term containing $-z - z_0 + 2p$. For $p = 0$ we have to sum over the four combinations of $\pm z \pm z_0$, while for $|p| = 1, 2 \dots$ we sum

over the eight combinations of $\pm z \pm z_0 \pm 2p$. Taking this into account, we find with the Poisson sum formula that with initial condition (75) the evolution is

$$a_0^\pm(x, y, z; t|z_0) = e^{-\frac{1}{2}r^2 - it} \frac{\partial^2}{\partial z_0^2} \left\{ \sum_{p=-\infty}^{+\infty} e^{i|z \pm z_0 - 2p|} \int_0^\infty J_0(r(ia|z \pm z_0 - 2p| + ias)^{1/2}) J_0(r(ias)^{1/2}) e^{2ias} ds \right\}. \quad (\text{B } 10)$$

As s runs from 0 to ∞ in the integrals, we see with (B 2) that the variable ias runs in the complex plane from zero to infinity in the lower left quadrant. Inspection of the asymptotic behaviour of the Bessel functions as the complex argument goes to infinity with s increasing, shows that the integrands vanish for $s \rightarrow \infty$ and that these integrals are convergent. We can rotate the line of integration to one running along the real axis from 0 to $-\infty$. Introducing the variable $x = -ias$ the integrals become

$$\int_0^\infty J_0(\dots) J_0(r(ias)^{1/2}) e^{2ias} ds = \frac{-1}{ia} \int_0^\infty J_0(\dots) I_0(rx^{1/2}) e^{-2x} dx, \quad (\dots) = r(ia|z \pm z_0 - 2p| - x)^{1/2}. \quad (\text{B } 11)$$

We have used here that $J_0(iz) = I_0(z)$ (Watson 1966).

REFERENCES

- CAHN, A. 1945 An investigation of the free oscillations of a simple current system. *J. Met.* **2**, 113–119.
- CARRIER, G. F., KROOK, M. & PEARSON, C. E. 1966 *Functions of a Complex Variable*. McGraw-Hill.
- FU, L. L. 1981 Observations and models of inertial waves in the deep ocean. *Rev. Geophys. Space Phys.* **19**, 141–170.
- GILL, A. E. 1982 *Atmosphere-Ocean Dynamics*. Academic Press.
- GILL, A. E. 1984 On the behavior of internal waves in the wake of storms. *J. Phys. Oceanogr.* **14**, 1129–1151.
- GREATBATCH, R. J. 1983 On the response of the ocean to a moving storm: the nonlinear dynamics. *J. Phys. Oceanogr.* **13**, 357–367.
- GREATBATCH, R. J. 1984 On the response of the ocean to a moving storm: parameters and scales. *J. Phys. Oceanogr.* **14**, 59–78.
- HASSELMANN, K. 1970 Wave-driven inertial oscillations. *Geophys. Fluid Dyn.* **1**, 463–502.
- KLOOSTERZIEL, R. C. 1990 On the large-time asymptotics of the diffusion equation on infinite domains. *J. Engng Maths* **24**, 213–236.
- KUNDU, P. K. 1993 Internal waves generated by traveling wind. *J. Fluid Mech.* **254**, 529–559.
- KUNDU, P. K. & THOMSON, R. E. 1985 Inertial oscillations due to a moving front. *J. Phys. Oceanogr.* **15**, 1076–1084.
- MORSE, P. M. & FESHBACH, H. 1953 *Methods of Theoretical Physics*. McGraw-Hill.
- POLLARD, R. T. 1970 On the generation by winds of inertial waves in the ocean. *Deep Sea Res.* **17**, 795–812.
- PRESS, W. H., FLANNERY, B. P., TEUKOLSKY, S. A. & VETTERLING, W. A. 1990 *Numerical Recipes: the Art of Scientific Computing*. Cambridge University Press.
- PRICE, J. F. 1983 Internal wave wake of a moving storm. Part 1: scales, energy budget and observations. *J. Phys. Oceanogr.* **13**, 949–965.
- RUBENSTEIN, D. M. 1983 Vertical dispersion of inertial waves in the upper ocean. *J. Geophys. Res.* **88**, 4368–4380.
- WATSON, G. M. 1966 *Theory of Bessel Functions*. Cambridge University Press.